Eur. Phys. J. D (2014) 68: 369
DOI: 10.1140/epjd/e2014-50643-y

THE EUROPEAN PHYSICAL JOURNAL D

Regular Article

Triple differential cross sections for the ionization of water by electron impact*

Istvan Tóth[1,a], Ladislau Nagy[1], and Radu I. Campeanu[2]

[1] Faculty of Physics, Babeş-Bolyai University, 400084 Cluj-Napoca, Romania
[2] Department of Physics and Astronomy, York University, 4700 Keele Street, Toronto, M3J 1P3, Canada

Received 29 August 2014 / Received in final form 23 September 2014
Published online 11 December 2014 –

Abstract. Calculated triple differential cross sections are presented for the ionization of the $3a_1$ orbital of water by electron impact. The cross sections are determined for symmetric coplanar and non-coplanar geometrical arrangements. The obtained results show reasonable agreement with experimental data for both geometries.

1 Introduction

The interaction of charged particles with matter is of interest for several research fields, like astrophysics, radiobiology, atmospheric sciences and even medical sciences. Water is one of the most abundant molecules on earth. It is largely present in biological tissues, therefore it is regarded as a test case for the interaction of charged particles with living tissues.

The ionization of water by electron impact has attracted much interest lately [1–6]. In fact, a growing interest concerning the ionization of molecular targets in $(e, 2e)$ processes has been observed. Such processes are described in terms of the TDCS (triple or fully differential cross section), which provides the angular distribution of the ejected electron of a given energy and for fixed momenta of the incident and scattered particles. Studies concerning the ionization of molecules are less abundant than for atomic targets due to the increased difficulties which arise when treating such complex structures. Experimentally is very difficult for example to separate the contributions of the electronic states with close energies, while for the theoretical treatment is challenging to take into account the multi-center nature of the targets. The investigated targets range from simpler molecules like H_2 [7–11], O_2 [12], N_2 [13–16] to more complex targets as CO_2 [17], CH_4 [18–23], NH_3 [24] or C_4H_8O [25].

In the present study we investigate the ionization of water by electron impact in coplanar, perpendicular and other non-coplanar geometrical arrangements. The TDCSs are determined for the $3a_1$ orbital of the H_2O molecule and for equal and non-equal energy sharing of the outgoing electrons. We consider a low-energy regime, the highest energy employed being equal to 20 eV. For all studied cases the electrons are emitted symmetric relative to the incident direction. Previously, we have performed TDCS calculations for the ionization of water, but for intermediate energies [3]. Similarly, we performed low-energy calculations for H_2 [11], but only in the perpendicular plane. Now, we intend to test the validity of our models for low energies also in case of the water molecule, both for coplanar and non-coplanar geometries. For such low energies of the outgoing particles, the PCI (post-collision interaction) effects may play a significant role. We incorporate these effects in our approach through the Coulomb distortion factor or the so-called Gamow factor of [26].

The TDCSs are calculated within the DWBA (distorted-wave Born approximation) formalism. In our approach, the continuum states of the free electrons are approximated by distorted waves, while the initial state of the molecular target is described by Gaussian type multicenter wavefunctions. The Gaussian molecular orbitals are constructed as linear combination of atomic-like orbitals. The atomic orbitals are given in terms of contracted Gaussian primitives. The molecular orbital coefficients were determined employing the Gaussian package [27].

The obtained results are compared with the experimental data and MDW (molecular distorted wave) theoretical results presented in reference [4]. Although, the MDW model contains PCI only to the first order of perturbation theory, in most cases provided better agreement with the experimental data in reference [4] compared to the M3DW (molecular three-body distorted wave) model [4].

* Contribution to the Topical Issue "Elementary Processes with Atoms and Molecules in Isolated and Aggregated States", edited by Friedrich Aumayr, Bratislav Marinkovic, Stefan Matejcik, John Tanis and Kurt H. Becker.

[a] e-mail: itoth@phys.ubbcluj.ro

2 Theory

The theoretical background employed here was described elsewhere [21], therefore we present only an outline of the theory.

The TDCS for the ionization of a molecular target in the framework of the DWBA method, in atomic units is given by:

$$\frac{d^3\sigma}{d\hat{\mathbf{k}}_f d\hat{\mathbf{k}}_e dE_e} = 2(2\pi)^4 \frac{k_f k_e}{k_i} |t|^2 , \quad (1)$$

where $\mathbf{k}_f$, $\mathbf{k}_e$ and $\mathbf{k}_i$ are the wave-vectors of the scattered, ejected and incident electrons, respectively. The energy of the ejected electron is denoted by E_e, while t stands for the transition matrix element of the system. The factor 2 in the expression above reflects the fact that an orbital is occupied by two electrons, and each of them can be active. For the direct ionization process, the transition matrix element of the system is t_d, which may be written as

$$t_d = \left\langle \phi_f(\mathbf{r}_1)\phi_e(\mathbf{r}_2) \left| -\frac{Z}{r_{12}} \right| \phi_b(\mathbf{r}_2,\alpha,\beta,\gamma)\phi_i(\mathbf{r}_1) \right\rangle . \quad (2)$$

In the above expression $Z = -1$ is the charge of the projectile, r_{12} stands for the distance between the projectile and the active target electron. The ϕ symbols with different subscripts denote the wavefunctions for the incident (i), bound (b), scattered (f) and ejected (e) particles, respectively. The bound electron wavefunction depends on the molecular orientation expressed by the Euler angles (α,β,γ). In order to separate the dependencies of these wavefunctions on the radial and angular coordinates, several expansions are performed. The wavefunctions of the scattered, ejected and incident electrons are expanded into partial wave series. The interaction between the projectile and the active electron is expanded into the multipole series as shown below:

$$\frac{1}{r_{12}} = \sum_{\lambda} \frac{4\pi}{2\lambda+1} \frac{r_<^{\lambda}}{r_>^{\lambda+1}} \sum_{\mu} Y_{\lambda\mu}(\hat{\mathbf{r}}_1) Y^*_{\lambda\mu}(\hat{\mathbf{r}}_2) . \quad (3)$$

The bound molecular wavefunction $\phi_b(\mathbf{r}_2,\alpha,\beta,\gamma)$ is expanded in terms of the spherical harmonics in the molecular frame as in [28], then the spherical harmonics are transformed into the laboratory frame by using the Wigner $D(\alpha,\beta,\gamma)$ functions, leading to the expression

$$\phi_b(\mathbf{r}_2,\alpha,\beta,\gamma) = \sum_{l_b m_b} Y_{l_b m_b}(\hat{\mathbf{r}}_2) \sum_{\nu} c_{l_b\nu}(r_2) D^{l_b}_{m_b\nu}(\alpha,\beta,\gamma). \quad (4)$$

Here $c_{l_b\nu}(r_2)$ are the expansion coefficients.

The direct matrix element is calculated similarly as in reference [21]. Since the above expression of the transition matrix element is given for a fixed orientation of the molecule, we average the cross section (1) over the Euler angles, using the expression

$$\int_0^{2\pi}\int_0^{\pi}\int_0^{2\pi} D^{*l'_b}_{m'_b\nu'}(\alpha,\beta,\gamma) D^{l_b}_{m_b\nu}(\alpha,\beta,\gamma) \mathrm{d}\alpha \sin\beta \mathrm{d}\beta \mathrm{d}\gamma = \frac{8\pi^2}{2l_b+1} \delta_{l_b l'_b} \delta_{m_b m'_b} \delta_{\nu\nu'} . \quad (5)$$

The exchange effects between the ejected and scattered electrons are taken into account by introducing an exchange term into the total transition matrix element

$$|t|^2 = |t_d|^2 + |t_{ex}|^2 - |t_d|\,|t_{ex}| . \quad (6)$$

Here the maximum interference is assumed. The exchange term is given by:

$$t_{ex} = \left\langle \phi_e(\mathbf{r}_1)\phi_f(\mathbf{r}_2) \left| -\frac{Z}{r_{12}} \right| \phi_b(\mathbf{r}_2,\alpha,\beta,\gamma)\phi_i(\mathbf{r}_1) \right\rangle , \quad (7)$$

where the coordinates of the ejected and scattered particles were exchanged relative to the direct matrix element (2).

We have calculated the TDCS with two methods, TS (total screening) and TS*, respectively. Both models use distorted waves in order to describe the continuum states.

In the TS model the ejected electron moves in the spherically averaged potential field of the nuclei screened by the spherically averaged field of the residual electrons (V_e), while the scattered electron experiences the effect of the spherically averaged nuclear potential and the field created by the electrons of the target (V_f):

$$\begin{cases} V_e = V_{nuclei} + V^-_{electrons} \\ V_f = V_{nuclei} + V_{electrons}. \end{cases} \quad (8)$$

The TS* model is a modified version of the TS. It assumes that both outgoing electrons move in the same potential field, i.e. in the spherically averaged potential of the residual ion:

$$V_e = V_f = V_{nuclei} + V^-_{electrons}. \quad (9)$$

V_{nuclei}, $V^-_{electrons}$ and $V_{electrons}$ stand for the spherically averaged potential of the nuclei, residual electrons and target electrons, respectively. The averaging method employed here was described elsewhere [29]. We mention that the spherical averaging of the nuclear potential results in the distribution of the nuclear charge on a sphere with the radius equal to the distance between the center of the molecule and the particular nucleus.

In both models the incident projectile moves in the spherically averaged potential of the nuclei and all electrons of the target (V_i):

$$V_i = V_{nuclei} + V_{electrons}. \quad (10)$$

The PCI effects are taken into account in our calculations through the so-called CDF (Coulomb distortion factor):

$$CDF = G \left|{}_1F_1\left(i\gamma, 1, -2ik_{fe} r_{fe}^{ave}\right)\right|^2 \quad (11)$$

where

$$G = \frac{\pi \exp(-\pi/k_{fe})}{k_{fe}[1-\exp(-\pi/k_{fe})]} \quad (12)$$

is called the Gamow factor. In the above equations ${}_1F_1$ is a confluent hypergeometric function, $k_{fe} = \mu v_{fe}$ and $\gamma = 1/v_{fe}$ is the Sommerfeld parameter. Here, v_{fe} stands for the relative velocity between the two electrons, while

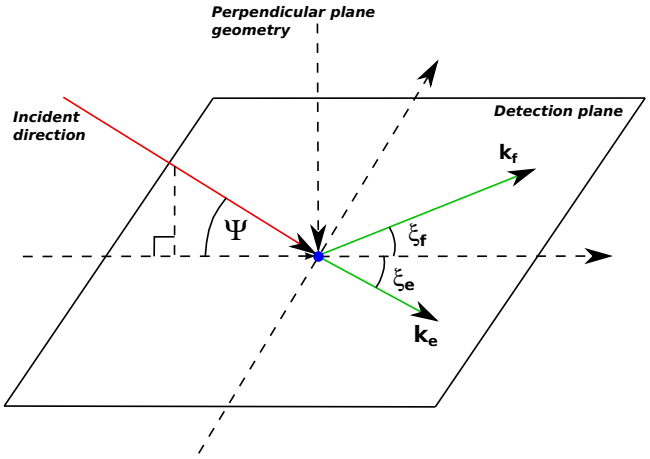

Fig. 1. The scattering geometry is defined by the Ψ angle. The outgoing electrons are detected at angles $\xi_f = \xi_e = \xi$.

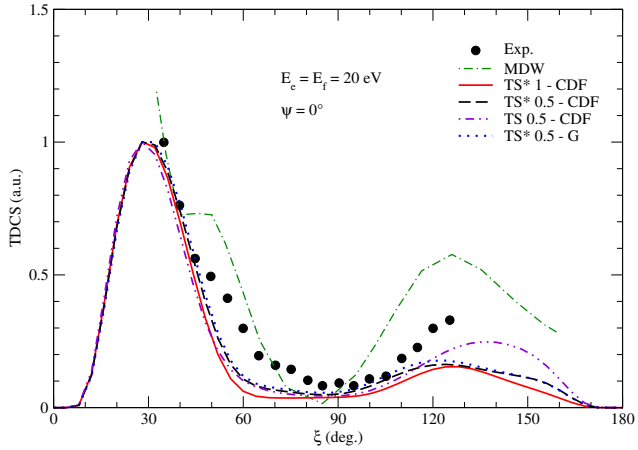

Fig. 2. TDCSs for the ionization of the $3a_1$ orbital of water by electron impact in the scattering plane. The TDCSs are plotted as a function of the ejection angle ξ. The energies of the outgoing electrons are $E_f = E_e = 20$ eV. The experimental points and the MDW results are from [4].

$\mu = 1/2$ is the reduced mass of the electrons. In (11) r_{fe}^{ave} is taken to be parallel to $\mathbf{k}_{fe}$ and is an averaged version of the actual electron-electron separation in the final state, $\mathbf{r}_{fe}$. The average separation is given by:

$$r_{fe}^{ave} = \frac{\pi^2}{16\epsilon_t}\left(1 + \frac{0.627}{\pi}\sqrt{\epsilon_t}\ln\epsilon_t\right)^2, \qquad (13)$$

where ϵ_t is the total energy of the scattered and ejected electrons. Using the averaged separation in (11) the TDCS (1) may be multiplied by the CDF factor. For further details see [26,30].

3 Results

Theoretical TDCSs for the ionization of water by electron impact are presented. The calculations have been performed for coplanar, perpendicular and other non-coplanar geometries. The geometrical arrangements are shown in Figure 1. The figure shows that a particular geometry is defined by the Ψ angle. If $\Psi = 0°$, a coplanar geometry is defined in a plane called the scattering plane. A perpendicular geometry is considered when $\Psi = 90°$. Between these two extremes other non-coplanar geometries may be obtained for various values of the Ψ angle. Figure 1 also shows that the outgoing electrons are emitted symmetrically relative to the incident beam direction. The ejection angles are denoted as ξ_f and ξ_e, for the scattered and ejected electron, respectively. These angles are taken to be equal ($\xi_f = \xi_e = \xi$) for all geometrical arrangements presented below.

We have investigated the ionization from the $3a_1$ orbital of water. The ionization energy of this orbital is 14.7 eV. Our results were obtained using two methods, TS and TS*. Cross sections have been determined also for a modified nuclei-ejected electron interaction. By averaging the nuclear potential, the charge of the different nuclei of the molecule will be distributed on a sphere, with a radius (R_0) which equals the distance from the molecular center to the particular nucleus. By reducing the radius with a given fraction n, the nuclei-electron interaction may be changed and the new radius becomes $R = n \times R_0$. The numbers in the figure legends represent the values of the fraction n. The spherically averaged nuclear potential may lead to a weak nuclei-electron interaction and consequently to a smaller intensity of the angular distribution at higher ejection angles in the scattering plane. In order to enhance this interaction, we reduce the radius of the sphere on which the nuclear charge is located. The enhancement of the nuclear potential led previously to a better description of the TDCS at high ejection angles, see [21] for example. However, the TDCSs in reference [21] were determined for higher energies and different kinematical parameters compared to the present calculations.

The calculations are performed for a low-energy regime. The energies of the scattered and ejected electrons are equal or lower than 20 eV, respectively. In such circumstances, it is expected that PCI effects to have an important impact on the calculated data. Our models take into account these effects through the Coulomb distortion factor (11) or simply the Gamow factor (12). The TDCSs calculated using these factors are denoted in the figure legends by CDF or G, respectively.

The results are compared with the experimental data and the MDW results from [4]. The experimental data are given on a relative scale, therefore we have normalized all TDCSs to unity at the highest peak location.

3.1 Scattering plane

Figures 2–7 show the results obtained for a coplanar geometry. Here, the cross sections are presented for equal (Figs. 2–5) and non-equal (Figs. 6 and 7) energy sharing of the scattered and ejected electrons. The TDCSs are shown as a function of the ejection angle ξ. The values

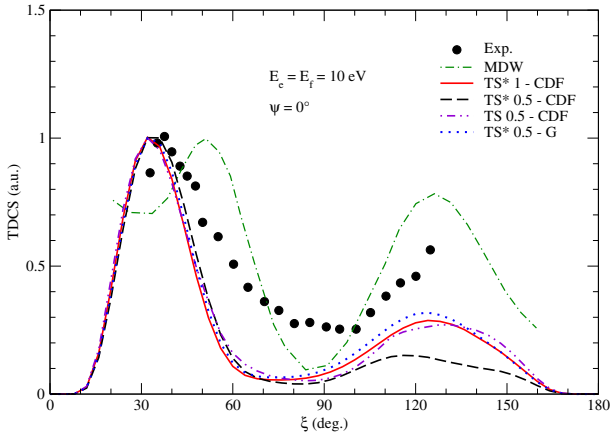

Fig. 3. Same as Figure 2, but for $E_f = E_e = 10$ eV.

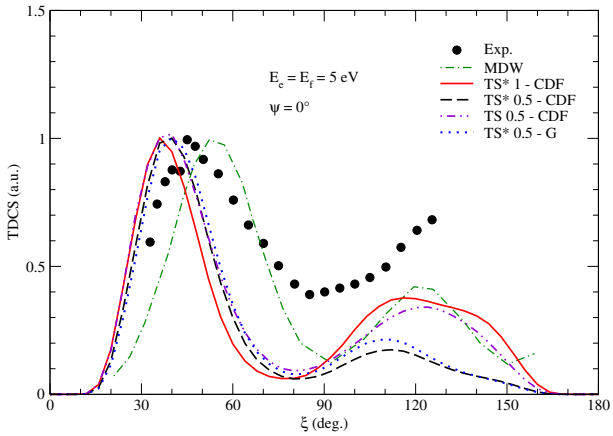

Fig. 4. Same as Figure 2, but for $E_f = E_e = 5$ eV.

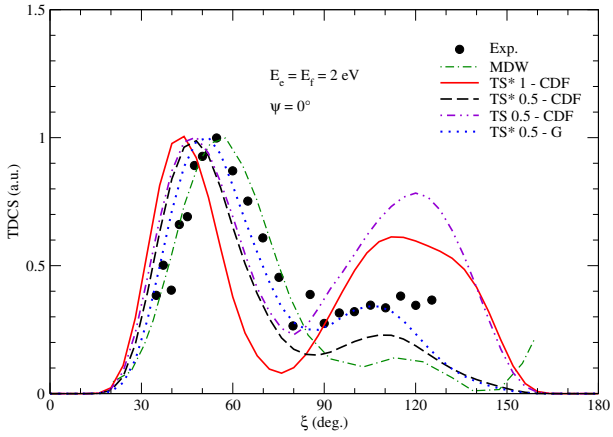

Fig. 5. Same as Figure 2, but for $E_f = E_e = 2$ eV.

of E_e and E_f range from 20 eV to 2 eV, as shown in the figures.

The experimental data show a typical behavior for a TDCS. A forward and a backward peak are observed at angles lower and higher than $\xi = 90°$, respectively. In all cases the intensity at smaller angles appears to be higher than for the large-angle region, although at high scattering

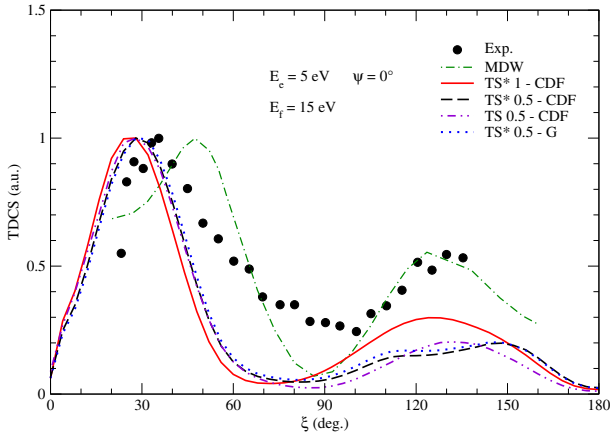

Fig. 6. Same as Figure 2, but for $E_f = 15$ eV and $E_e = 5$ eV.

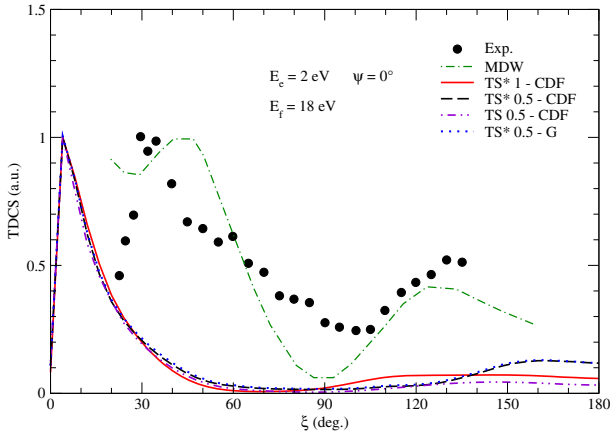

Fig. 7. Same as Figure 2, but for $E_f = 18$ eV and $E_e = 2$ eV.

angles there are no experimental data, therefore it is difficult to make assessments for the behavior of the TDCS.

For equal energy sharing of the outgoing electrons, in Figures 2–5, our models show good agreement with the experimental data, especially in the small-angle region and for high energies. At high energies, all models give the same position for the forward peak. As the energy is decreasing, the maxima of the different TS and TS* models appear slightly shifted relative to each other. The models reproduce the shift of the experimental forward peak towards higher ξ angles as the energy becomes smaller. This effect is more likely due to the PCI, which at low and equal energies becomes more important. The experimental backward peak shows increasing tendency with decreasing ejection energies except for $E_f = E_e = 2$ eV. As the energy of the outgoing electrons becomes smaller, they interact longer with each other, but they also have more time to interact with the nuclear core, therefore an enhanced nuclei-electron interaction is expected to lead to a larger backward intensity. This behavior is nicely reproduced for example by the (TS*1-CDF) model for the whole energy range. This model also predicts a shift of the backward peak towards $\xi = 90°$ as the energy takes smaller values, which again, may be the consequence of PCI effects.

At the lowest energy ($E_f = E_e = 2$ eV), the best agreement with the experiment seems to be provided by the (TS*0.5-G) model. At higher energies the MDW model shows a forward peak at higher angles than our models and the experimental data, however, at low energies agrees well with the experiment. The position of the backward peak is predicted both by the MDW and our models to be around the same angle.

We observe in Figures 2–5 that only at the highest energy the enhancement of the nuclear potential (see the (TS*1-CDF) and (TS*0.5-CDF) models) leads to a slightly higher intensity for large ejection angles. At low energies the PCI effect becomes stronger, which may modify the behaviour of the TDCS at high ejection angles.

In Figures 6 and 7, we present cross sections for unequal energy sharing of the electrons. In this case the scattered and ejected electrons have a total excess energy above the ionization energy of 20 eV. Figure 6 shows the case when $E_e = 5$ eV and $E_f = 15$ eV. In Figure 7 the $E_e = 2$ eV and $E_f = 18$ eV case is depicted. While in Figure 6 our models show some agreement with the experiment, in Figure 7 our models severely underestimate the position of the forward peak and show no intensity at all for high angles. Nevertheless, some similarity may be observed concerning the shape of the forward peak. Both the experimental and the calculated peaks are very narrow. The precise cause of the discrepancy is not known.

Starting from a symmetric energy sharing case in Figure 3 and gradually increasing the asymmetry of the shared energy in Figures 6 and 7, we observe that the position of the experimental forward peak gradually moves toward smaller angles. This behavior may be observed also in case of our calculated data (see for example the (TS*1-CDF) model. For non-equal energy sharing the MDW model provides a very good agreement at the large-angle region with the experimental data, but gives higher angles for the position of the forward peak.

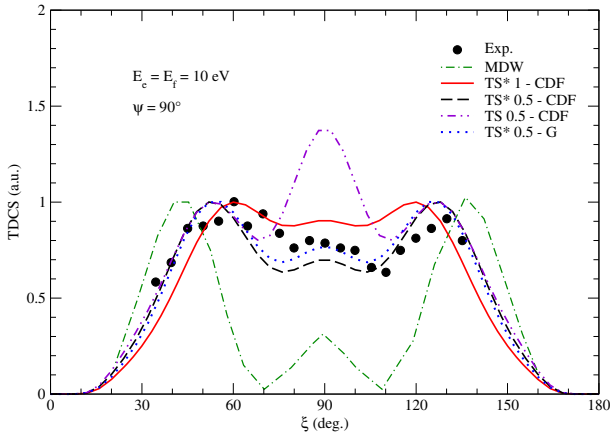

Fig. 8. TDCSs for the ionization of the $3a_1$ orbital of water by electron impact in the perpendicular plane. The TDCSs are plotted as a function of the angle ξ. The energies of the outgoing electrons are $E_f = E_e = 10$ eV. The experimental points and the MDW results are from [4].

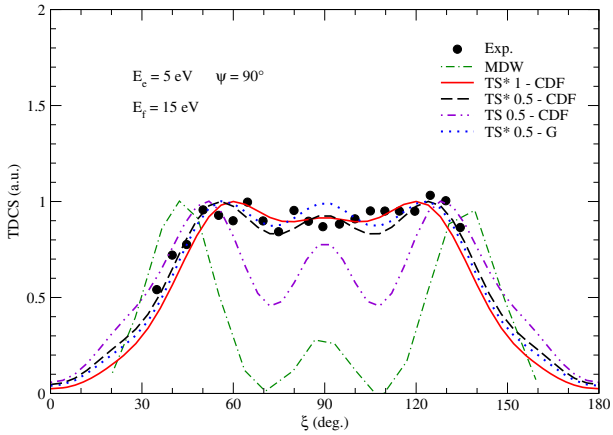

Fig. 9. Same as Figure 8, but for $E_f = 15$ eV and $E_e = 5$ eV.

3.2 Perpendicular plane

The results obtained for a perpendicular geometry are plotted in Figures 8–10. We start from a symmetric energy sharing of the outgoing electrons and gradually increase the asymmetry of the shared energy.

The experimental TDCS shows almost no change in its structure as the energy sharing is changing from a symmetric case to an asymmetric one. It shows an almost constant angular distribution, except for low and high angles. However, in Figure 8, where $E_f = E_e = 10$ eV, some small structures may be observed. Our models provide similar cross sections, except for the (TS 0.5-CDF) model, which shows a triple peak structure, with a dominant central peak, which overestimates the experimental data. The agreement appears to be the best in case of the other two (TS* 0.5) models.

For $E_e = 5$ eV and $E_f = 15$ eV, in Figure 9, a similar situation is observed. Our models seem to be in good agreement with the experimental data and show similar cross sections, except for the (TS 0.5-CDF) model. Now, the central peak of this model is smaller than the flanking peaks, but still large compared to the experimental data.

At the highest asymmetry, when $E_e = 2$ eV and $E_f = 18$ eV, the (TS 0.5-CDF) model shows again significant disagreement with the experiment. The best agreement appears to be in case of the (TS* 1-CDF) model. Despite this agreement, our models show some important differences compared to the above cases. At low and high angles, the TDCSs calculated in our models show significant intensities. This can be explained by a smaller repulsion of the electrons moving in the same direction, having different energies.

We note that the MDW model shows a triple-peak structure and almost identical cross sections in all cases.

3.3 Other non-coplanar geometries

We have calculated TDCSs also for a symmetric energy sharing case ($E_f = E_e = 10$ eV), but for different non-coplanar geometrical arrangements. These results are

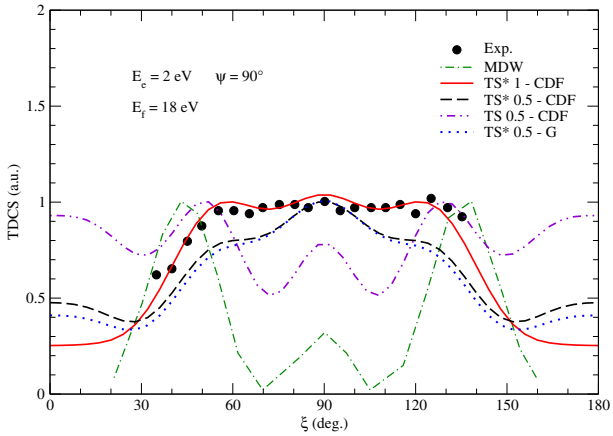

Fig. 10. Same as Figure 8, but for $E_f = 18$ eV and $E_e = 2$ eV.

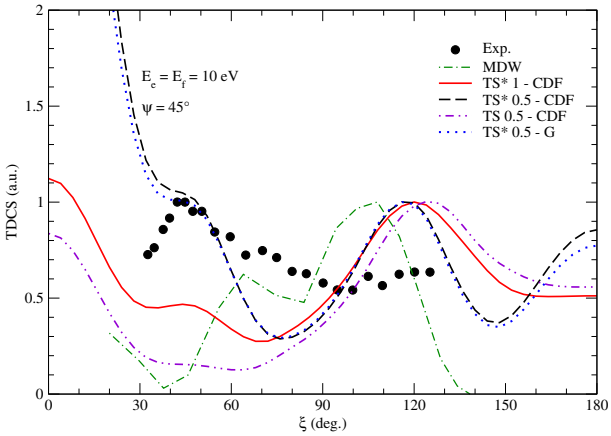

Fig. 12. Same as Figure 11, but for $\Psi = 45°$.

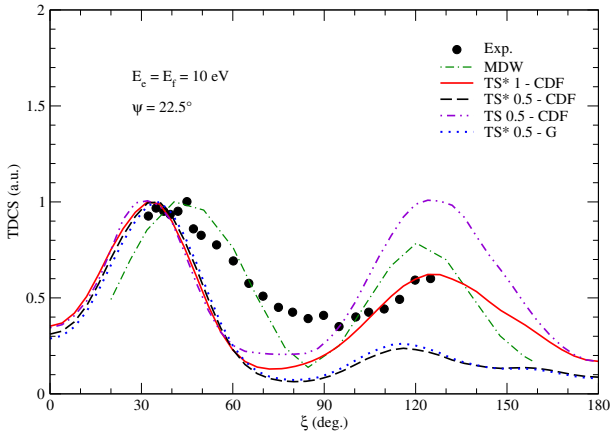

Fig. 11. TDCSs for the ionization of the $3a_1$ orbital of water by electron impact and for $\Psi = 22.5°$. The TDCSs are plotted as a function of the angle ξ. The energies of the outgoing electrons are $E_f = E_e = 10$ eV. The experimental points and the MDW results are from [4].

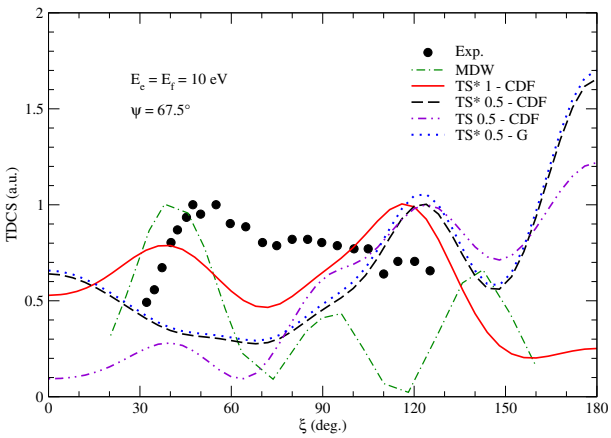

Fig. 13. Same as Figure 11, but for $\Psi = 67.5°$.

presented in Figures 11–13, for $\Psi = 22.5°$, 45°, and 67.5°, respectively.

The experimental data show an increasing intensity at large angles compared to the low-angle region as the electron-gun angle Ψ is increasing. The difference between our models and the experiment is increasing for larger Ψ angles. However, the best agreement is provided by the (TS*1-CDF) model.

4 Conclusions

We have determined TDCSs for the ionization of water by electron impact. The calculations were performed for a coplanar and several non-coplanar geometries, including the perpendicular geometry. In the scattering and perpendicular planes, the ionization have been studied for equal and non equal energy sharing of the outgoing electrons.

In a coplanar geometry and for equal energy sharing of the electrons, our models show better agreement with the experiment at higher energies and especially at the forward peak position. The models are able to reproduce some qualitative features of the experimental cross section. One of these features is the migration of the forward peak towards larger ejection angles as the energy is decreasing. This behavior is the consequence of the PCI effects between the emitted electrons. Some of the employed models show an increasing intensity at the backward peak location with decreasing electron energy, which may be the effect of an enhanced nuclei-electron interaction at lower energies. The TDCSs calculated with the Coulomb distortion factor and the Gamow factor proved to be very similar, especially at higher energies. At lower energies the Gamow data seemed to be more accurate.

As the energy is flipped from a symmetric energy sharing to an increasing asymmetry in the energy share between the outgoing particles, the forward peak was observed to move toward lower ejection angles. Nevertheless, the agreement with the experimental data becomes less satisfactory with increasing asymmetry in energy sharing.

In the perpendicular plane our calculated cross sections show a very good agreement with the experimental data. For an increasing asymmetry in the energy sharing of the outgoing electrons, the experimental TDCS shows an almost constant angular distribution. Nevertheless, at the highest asymmetry, our models provided significant

intensity in the calculated data for low and high angles, which was not observed for lower asymmetry or in the symmetric case.

The calculated cross sections for other non-coplanar geometrical arrangements show better agreement with the experimental data at lower gun-angles.

This work was supported by a grant of the Romanian National Authority for Scientific Research, CNCS-UEFISCDI, project No. PN-II-ID-PCE-2011-3-0192 (L. Nagy) and by a grant of the Babeş-Bolyai University, project No. GTC34032/2013 (I. Tóth).

References

1. C. Champion, C. Dal Cappello, S. Houamer, A. Mansouri, Phys. Rev. A **73**, 012717 (2006)
2. C. Champion, Phys. Med. Biol. **55**, 11 (2010)
3. I. Tóth, R.I. Campeanu, L. Nagy, Eur. Phys. J. D **66**, 21 (2012)
4. K.L. Nixon et al., J. Phys. B **43**, 035201 (2010)
5. M. Sahlaoui, M. Bouamoud, B. Lasri, M. Dogan, J. Phys. B **46**, 115206 (2013)
6. C.Y. Lin, C.W. McCurdy, T.N. Rescigno, Phys. Rev. A **89**, 012703 (2014)
7. E.M. Staicu Casagrande et al., J. Phys. B **41**, 025204 (2008)
8. A. Senftleben et al., J. Phys. B **45**, 021001 (2012)
9. O. Al-Hagan et al., Phys. Rev. A **81**, 030701(R) (2010)
10. O. Al-Hagan et al., Nat. Phys. **5**, 59 (2008)
11. I. Tóth, L. Nagy, V. Chiş, L. Gulyás, Eur. Phys. J. D **66**, 313 (2012)
12. J. Yang, J.P. Doering, Phys. Rev A **63**, 032717 (2001)
13. J.P. Doering, J. Yang, Phys. Rev A **60**, 2176 (1999)
14. A. Naja et al., J. Phys. B **40**, 3775 (2007)
15. A. Lahmam-Bennani, E.M. Staicu Casagrande, A. Naja, J. Phys. B **42**, 235205 (2009)
16. A.J. Murray, M.J. Hussey, J.F. Gao, D.H. Madison, J. Phys. B **39**, 3945 (2006)
17. M.J. Hussey, A.J. Murray, J. Phys. B **38**, 2965 (2005)
18. A. Lahmam-Bennani et al., J. Phys. B **42**, 165201 (2009)
19. K.L. Nixon et al., J. Chem. Phys. **134**, 174304 (2011)
20. K.L. Nixon et al., J. Chem. Phys. **136**, 094302 (2012)
21. I. Tóth, L. Nagy, J. Phys. B **43**, 135204 (2010)
22. H. Chaluvadi, C.G. Ning, D.H. Madison, Phys. Rev. A **89**, 062712 (2014)
23. C.Y. Lin, C.W. McCurdy, T.N. Rescigno, Phys. Rev. A **89**, 052718 (2014)
24. K.L. Nixon et al., J. Chem. Phys. **138**, 174304 (2013)
25. C.J. Colyer et al., J. Chem. Phys. **133**, 124302 (2010)
26. S.J. Ward, J.H. Macek, Phys. Rev. A **49**, 1049 (1994)
27. M.J. Frisch et al., *Gaussian09, Revision A.2* (Gaussian, Inc., Wallingford, CT, 2009)
28. R.I. Campeanu, V. Chiş, L. Nagy, A.D. Stauffer, Nucl. Instrum. Methods B **247**, 58 (2006)
29. I. Tóth, R.I. Campeanu, V. Chiş, L. Nagy, Phys. Lett. A **360**, 131 (2006)
30. D.H. Madison, O. Al-Hagan, J. At. Mol. Opt. Phys **2010**, 367180 (2010)